



Amino-functionalized zirconium and cerium MOFs: Catalysts for visible light induced aerobic oxidation of benzylic alcohols and microwaves assisted *N*-Alkylation of amines

Antonio Valverde-González^a, Mercedes Pintado-Sierra^b, Antonia Rasero-Almansa^a, Félix Sánchez^{b,*}, Marta Iglesias^{a,*}

^a Instituto de Ciencia de Materiales de Madrid, ICMM-CSIC, C/ Sor Juana Inés de la Cruz, 3, Madrid, Spain

^b Instituto de Química Orgánica General, IQOG-CSIC, C/ Juan de la Cierva, 3, Madrid, Spain

ARTICLE INFO

Keywords:

Amino linker
Zirconium MOF
N-alkylation of amines
Photocatalytic oxidation
Microwaves activation

ABSTRACT

Herein we report that mixed zirconium-cerium-MOFs with amino-functionalized linkers (2-amino-1,4-benzenedicarboxylate, BDC-NH₂, and 4-aminonaphthalene-2,6-dicarboxylate, NDC-NH₂) act as effective non-noble-metal-based heterogeneous catalysts, for both the aerobic photooxidation of benzylic alcohols and for the direct microwaves activation *N*-alkylation of amines with alcohols. The catalytic performance has been studied considering two different approaches: the effect of NH₂ functionalized linkers and the effect of hosting Ce^{III} species on Zr-MOFs. Zr- and ZrCe-MOFs resulted efficient visible-light-driven photocatalysts with high stability and considerable recyclability in the photocatalytic selective oxidation of alcohols to aldehydes using molecular oxygen as oxidant. These materials are also effective catalysts for the microwaves-assisted *N*-alkylation of amines with alcohols yielding selectively the imine (ZrCe-MOF) or the corresponding secondary amine (Ce-MOFs).

1. Introduction

Metal organic frameworks (MOFs), consisted of inorganic nodes and organic linkers with high surface areas, are the class of materials that have aroused more interest among researchers in recent years [1,2]. The wide tunability of MOFs is due to the great variety of potentials linkers; metallic nodes that creates the framework and get organized into a periodic network [3]. It is possible to use this tunability to modify the electronic structure to afford specific catalytic reactions [4,5]. For example, MOF can influence on the catalytic behavior and it is important to identify catalytic centers, identify transport-reaction processes and control basic catalytic reaction rates [6–8]; there exist also appreciable number of MOFs as well-defined supports for homogeneous catalysts [9–11]. UiO-66 is a family of porous zirconium MOFs [Zr₆O₄(OH)₄(linker-CO₂)₁₂] with large surface area and pore volume and high thermal stability [12].

Cerium is the most abundant rare-earth element and compared with other lanthanides displays unique chemical properties. Cerium has +3 oxidation state typical of the lanthanide series and +4 oxidation state

because of its [Xe]4f¹5d¹6s² electron configuration. Both CeCl₃ (electron donor Lewis acid) and ceric ammonium nitrate (CAN) (electron acceptor strong oxidizing agent) have been broadly applied in organic synthesis [13,14]. The importance of ceria has been included on MOF research but compared to other metals the number of cerium MOFs reported remain low. Analogously to zirconium-based-MOFs, there are different crystalline networks with nodes formed by hexacerium(IV)-oxy clusters (Ce-Uio-66, Ce-MOF-808, Ce-MOF-545 and Ce-NU-1000, 1008, 1200) [15–17]. These Ce-MOFs have been applied as catalysts for different reactions: photochemical water splitting, redox, Lewis acid, hydroboration or hydrophosphination, acetalization processes [18–22] sensing [23] and gas absorption [24,25]. Recently, Ce-MOFs have been also applied as supports for vanadium homogeneous catalysts [26].

Introduction of different metal cations in MOFs provides an interesting strategy to tune the properties of porous materials towards practical applications. Mixed-metal MOFs may be synthesized by direct synthesis under solvothermal conditions, by post-synthesis metal exchange (PSE) [27], or by secondary building unit rational design [28]. In the literature, we can found mixed lanthanide frameworks with highly

* Corresponding author.

E-mail addresses: a.valverde.gonzalez@csic.es (A. Valverde-González), m.pintado@csic.es (M. Pintado-Sierra), felix-iqu@iqog.csic.es (F. Sánchez), marta.iglesias@icmm.csic.es (M. Iglesias).

<https://doi.org/10.1016/j.apcata.2021.118287>

Received 5 May 2021; Received in revised form 7 July 2021; Accepted 11 July 2021

Available online 14 July 2021

0926-860X/© 2021 The Author(s). Published by Elsevier B.V. This is an open access article under the CC BY license (<http://creativecommons.org/licenses/by/4.0/>).

tunable luminescent properties [29], and some examples of Ce(III) doped Zr-based MOFs for NO₂ adsorption [30], catalytic decomposition of methanol into CO₂ [31,32] and aerobic oxidation of benzyl alcohol have been also reported [17]. Cerium(IV) adopts eight coordination positions in its common oxide CeO₂ and is an attractive candidate for the substitution of Zr into UiO-66 derivatives. The properties of CeO₂-ZrO₂ solid solutions are well established in redox catalysis and for their oxygen storage properties [33].

In the last years, several reviews have summarized the application of MOFs as heterogeneous catalysts depending on the type of active site (metal, linker, etc.) or synthetic method [34–37]. In the specific case of oxidation reactions, selective oxidation of different organic products has been widely studied by their environmental consequences. To evaluate the activity of oxidation catalysts of MOFs, a model reaction is the selective oxidation of benzylic alcohols to the corresponding benzaldehyde [38,36,37]. MOFs are excellent multifunctional materials that can be applied for cascade reactions as the *N*-alkylation of amines with alcohols through several steps as alcohol oxidation, condensation with the amine yielding the imine and oxidation to the corresponding *N*-amine [39,40] and recently, it has been reported that NH₂-MIL-125 has an excellent catalyst for this reaction under solvent and base free conditions via borrowing hydrogen mechanism [41].

The use of amino-carboxylic acids as linkers to obtain amino-functionalized MOFs is mainly based on 2-amino-1,4-benzenedicarboxylate (BDC-NH₂) and their derivatives [42,43] and there are scarce examples with biphenyl- [44–46] and especially with naphthalene-based ligands [47–50]. Herein, we report the synthesis of mixed ZrCe-MOFs with BDC-NH₂ and a mix of naphthalene-2,6-dicarboxylate (NDC) and 4-aminonaphthalene-2,6-dicarboxylate (NDC-NH₂) linkers to modulate the surface charge of MOF networks and concurrently change the active sites incorporating redox centers [51]. Finally, we evaluated their behavior as photocatalysts for the aerobic oxidation of benzylic alcohols to aldehydes and towards the microwaves-assisted *N*-alkylation of benzyl alcohols with amines.

2. Experimental section

2.1. Synthesis of Zr-MOFs and bimetallic Zr(Ce)-MOFs

Pure Zr-MOF, Zr(BDC-NH₂) and Zr(NDC)(NDC-NH₂), were prepared as reported previously [31]. Mixed ZrCe-MOFs were prepared following the same method but modified as follows: A mixture of ZrCl₄ (466 mg, 2 mmol), CeCl₃·7H₂O (236 mg, 0.5 mmol) and 2.5 mmol of linker (BDC-NH₂, NDC or mixed NDC/NDC-NH₂ in a ratio 1/0.25) were dissolved in 12 mL of *N,N*-dimethylformamide (DMF) and placed in a Teflon lined vessel. The obtained mixture was heated at 393 K for 24 h. After cooling the solid was separated by centrifugation, and washed with 3 × 10 mL of DMF, 10 mL of MeOH and 10 mL of THF. The final solids were dried at 100 °C under vacuum to yield: Zr_{4.4}Ce_{1.6}O₄(OH)₄(C₈H₅NO₄)₆ (27 % of Ce functionalization and 100 % BDC-NH₂ linker), Zr_{4.9}Ce_{1.1}O₄(OH)₄(C₁₂H₈O₄) (18 % of Ce functionalization) and Zr_{4.5}Ce_{1.5}O₄(OH)₄(C₁₂H₈O₄)(C₁₂H₉NO₄)₅ (25 % of Ce functionalization and 25 % NDC-NH₂ linker).

2.2. Synthesis of Ce-MOFs

UiO-66-Ce(IV) MOF was prepared by the reported procedure with some modifications [17]: In a Pyrex glass tube naphthalene-2,6-dicarboxylate (NDC; 86.4 mg, 0.4 mmol) was dissolved into 4 mL of DMF, then 800 μL of a solution of ammonium cerium(IV) nitrate ((NH₄)₂Ce(NO₃)₆ 0.05 M, (219.2 mg, 0.4 mmol) was added and the reactor sealed. The mixture was sonicated for 20 min. The resulting solution was heated at 100 °C for 4 h. Finally, the white-yellowish powder was separated by filtration and washed with DMF, deionized water and ethanol, and dried at vacuum for 12 h at 60 °C to yield: Ce₆O₄(OH)₄(C₁₂H₈O₄)

FJU6-Ce(III) MOF was also prepared according to reported procedure [52]: In a Pyrex glass tube naphthalene-2,6-dicarboxylate (NDC; 92.4 mg, 0.416 mmol) was dissolved into 6 mL of DMF, then 800 μL of a solution of CeCl₃·7H₂O (115.10 mg, 0.416 mmol) was added and the reactor sealed. The mixture was sonicated for 20 min. The resulting solution was heated at 100 °C overnight. Finally, the white powder was separated by filtration and washed with DMF, deionized water and ethanol, and dried at vacuum for 12 h at 60 °C to yield: Ce₂(H₂O)(C₁₂H₈O₄)₃.

An alternative synthesis of FJU6-Ce(III) MOF is as follows: In a Pyrex glass tube naphthalene-2,6-dicarboxylate (NDC; 86.4 mg, 0.4 mmol) was dissolved into 4 mL of DMF, then 800 μL of a solution of ammonium cerium(IV) nitrate ((NH₄)₂Ce(NO₃)₆ 0.05 M, (219.2 mg, 0.4 mmol) was added. Then, 5 μL of H₂O₂ were added, what the solution to change color from orange to clear-white. The mixture was sonicated for 20 min and the reactor sealed. The resulting solution was heated at 100 °C overnight. Finally, the white powder was separated by filtration and washed with DMF, deionized water and ethanol, and dried at vacuum for 12 h at 60 °C to yield: Ce₂(H₂O)(C₁₂H₈O₄)₃.

2.3. Evaluation of catalytic activity

2.3.1. Photocatalytic oxidation of benzylic alcohols

The photocatalytic oxidation of benzyl alcohol as model was performed as follows. A mixture of alcohol (0.08 mmol) and 20 mg of photocatalyst in 1.5 mL of acetonitrile (ACN), previously saturated with oxygen was irradiated by a blue light emission diode (LED) (50 W, λ ≥ 420 nm, light-emitting spectrum is shown in Fig. S26). After the reaction, the mixture was separated from the reaction media and then washed with acetonitrile, ethyl acetate and diethyl ether. The reaction progress was analyzed by gas chromatography (GC).

2.3.2. *N*-alkylation of benzyl alcohols with amines

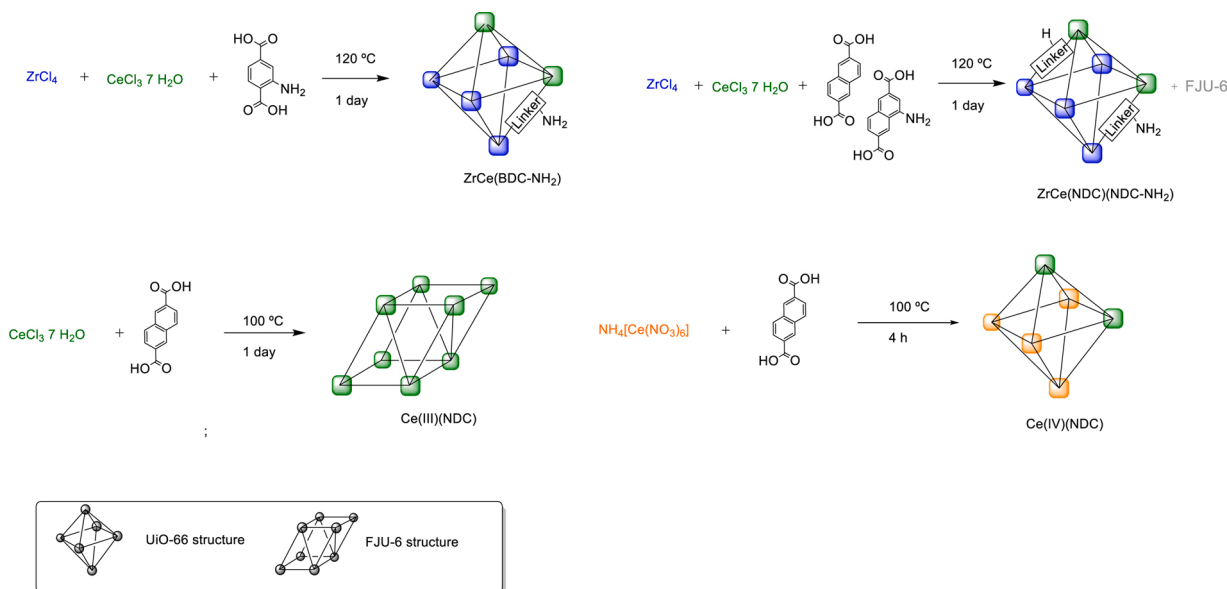
a) Zr-based-MOFs as catalysts: Benzyl alcohol (0.2 mmol) and the amine (0.1 mmol) were mixed in 0.5 mL of xylene and then, MOF catalyst (10 mg) was added to a microwave sealed-vessel equipped with a magnetic stirring bar. This flask was irradiated in a microwave synthesis reactor Anton Paar Monowave 300 at 120 °C for 8 h. Then, the catalyst is filtered and the products were analyzed by GC-MS.

b) Ce-MOFs as catalysts: Benzyl alcohol (0.2 mmol), the amine (0.1 mmol) and KO^tBu (0.1 mmol) were added to a microwave sealed-vessel equipped with a magnetic stirring bar and containing chlorobenzene (0.5 mL) and then, MOF catalyst (6 mg) was incorporated to the mixture. This flask was irradiated in a microwave synthesis reactor Anton Paar Monowave 300 at 120 °C for 3 h. At the end, the reaction products were analyzed by GC-MS.

3. Results and discussion

3.1. Synthesis and characterization

Zr- and mixed ZrCe-MOFs were prepared by direct synthesis under solvothermal conditions in a Teflon lined vessel at 120 °C for 24 h (Scheme 1) as described previously [31,47]. The reaction was performed with 2.5 mmol of the corresponding linker (BDC-NH₂, mixed NDC/NDC-NH₂), ZrCl₄ (2.0 mmol) and CeCl₃·7H₂O (0.5 mmol) in 12 mL of DMF at 120 °C for 24 h. The reaction mixture was filtered, and the resulting solids were thoroughly washed with DMF and MeOH to remove unreacted species. The procedure is shown in Scheme 1 and the prepared materials are collected in Table S1. The Zr and Ce loading were quantified by total reflection X-ray fluorescence (TXRF) spectrometry and corresponds to a metal composition of Zr_{4.4}Ce_{1.6} for ZrCe (BDC-NH₂), Zr_{4.9}Ce_{1.1} and Zr_{4.5}Ce_{1.5} for ZrCe(NDC)(NDC-NH₂). The amount of -NH₂ groups in the structure was calculated by elemental analysis of nitrogen (Table S1). ZrCe(BDC-NH₂) is only formed by amino-ligand whereas ZrCe(NDC)(NDC-NH₂) is composed from a mixed



Scheme 1. Direct synthesis of ZrCe- and Ce-MOFs.

of linkers with a ~25 % of amino-compound.

Fig. 1a shows the powder x-ray diffraction (PXRD) patterns of pure Zr(BDC-NH₂) compared to that of mixed ZrCe(BDC-NH₂). As can be observed the mixed MOF presents the typical UiO-66 phase with two main peak positions at 2θ 7.3, 8.4°. The same diffraction pattern (Fig. 2a) can be observed for Zr(NDC)(NDC-NH₂) and ZrCe(NDC)(NDC-NH₂), the two main peaks are slightly shifted due to the higher length of NDC ligand compared to BDC: 2θ 6.5 and 7.4°. Cerium loading's increase from 20 % to 75 % seems to affect the crystallinity of the UiO-66 structure by widening the two main peaks, as can be seen in Fig. S1. Moreover, the formation of a new phase with peaks at around $2\theta = 9.7$ and 9.9° is observed. Considering these data, from now on we will only study mixed MOFs obtained from a ~20 % of cerium loading, which mainly maintain the UiO-66 structure with both ligands.

To elucidate the new obtained phase with the NDC ligand, which is minority, we synthesized the corresponding pure Ce(NDC)-MOF. When CeCl₃·7H₂O was employed as cerium (III) precursor, a FJU-6 structure was obtained. However, if a cerium (IV) salt, NH₄[Ce(NO₃)₆] also known as CAN, was employed the UiO-66 topology was obtained, and showed a similar PXRD pattern to the reported for Zr(NDC)(NDC-NH₂)-UiO-66 [47] and Ce(IV)-UiO-66-MOFs [17].

Zr/Ce-UiO-66-BDC is by far the most studied family of Zr/Ce-MOFs and it can be concluded that these types of MOFs show a strong preference to form three types of clusters: Ce₆, Zr₆ and CeZr₅ [52–57]. Jacobsen et al. [58] based on Ce and Zr K-edge EXAFS analysis confirmed that up to a 16.7 % of Ce loading in the mixed MOF, Zr₆ and CeZr₅ clusters are observed, whereas at higher Ce loadings, only CeZr₅ and Ce₆ are present. Thus, based on our cerium loading, estimated by combination of elemental analysis and TXRF, (being 11.8 % for ZrCe(BDC-NH₂) and 9.3 % for ZrCe(NDC)(NDC-NH₂), Table S1) and the fact that our mixed MOF show a UiO-66 topology we could conclude that the clusters present in our MOFs are Zr₆ and CeZr₅. Besides, this preference to form CeZr₅ clusters is observed in MOF with different topologies, such as in Ce/Zr-CAU-38-PZDC [59], where this cluster was exclusively formed. This let us to conclude that the nature of the ligand does not seem to be determinant in this case, and we can hypothesize that BDC-NH₂, NDC and NDC-NH₂ do not modify the mixed cluster CeZr₅ formation.

Cerium (III)-MOF was characterized by powder and single crystal X-ray diffraction and as it can be observed in Fig. S2, the same phase previously reported by Chien et al. [60] was obtained. Cerium (IV)-MOF shows a powder X-ray diffraction pattern that agree with the typical reported for a UiO-66 structure (Fig. S2). As it has been previously

described, cerium (IV) based MOFs are unstable compared to cerium(III) and its preparation needed to be optimized, since depending on the reaction time and the water content it can be obtained pure cerium formate (by the hydrolysis of the DMF) and even its analogous cerium (III) MOF with FJU-6 topology (by *in situ* reduction of CAN). In our hands, the optimized reaction time to selectively obtained UiO-66 topology was 4 h using only 800 μ L of H₂O. We have also demonstrated that cerium (IV) can be employed as a FJU-6 MOF precursor in presence of H₂O₂ (since CAN is more oxidant than H₂O₂) when the same reaction was performed in presence of 2 equivalents of pure H₂O₂ a highly crystalline cerium(III) MOF with FJU-6 topology was obtained. These results agree with those reported in the literature since a linear dicarboxylate ligand (such as NDC) no cerium(IV) MOFs have been described with FJU-6 topology and no cerium(III) MOFs with UiO-66 structure.

Thermogravimetric analysis (TGA) (Figs. 1b and 2 b) shows that mixed MOFs are highly stable with a minor step at 100 °C because of a loss of adsorbed and lattice coordinated solvents, a second step at ~250 °C attributed to DMF and water coordinated in the pores of the framework, and the most important loss at ~400 °C (ZrCe(BDC-NH₂)) and 500 °C (ZrCe(NDC)(NDC-NH₂)) due to the decomposition of materials. Ce(III)(NDC)-FJU-6-MOF has a similar thermal stability with a first loss at ~200 °C due to the coordinated DMF molecules, resulting the Ce₂(NDC)₃ MOF [61], and the most important loss at 400 °C. However, Ce(IV)(NDC)-UiO-66 MOF is less stable and decomposes at 320 °C (see Fig. S3 for the TGAs of Ce MOFs). TGA analysis also served to correlate the metal loading of all MOFs by the residue and provides further information about the formation of mixed metal clusters, since as it has been described, the thermal stability decreases when the Ce loading increases [62,63].

FT-IR spectra show the characteristic $\nu(\text{CO})$ anti-symmetric at 1590–1550 cm⁻¹ and symmetric at 1434–1380 cm⁻¹, $\nu(\text{CC})$ and (CH) at 2930 cm⁻¹ frequencies, similar to that of the corresponding parent Zr-MOFs as can be observed in Figs. 1c and 2 c. Two peaks at ~3450, ~3375 cm⁻¹ are also observed, which are attributed to the asymmetrical and symmetrical stretching vibration adsorption of the NH₂ groups. Adsorption bands due to the adsorbed DMF (C=O, 1659 cm⁻¹) or water (OH, 3450 cm⁻¹) molecules are also observed. Moreover, weak bands due to $\nu(\text{Ce-O})$ appear at 460 and 668 cm⁻¹ [64]. Fig. S4 displays the FT-IR spectra of Ce MOFs showing the $\nu(\text{CO})$ band at 1600 cm⁻¹ and the characteristics Ce-O frequencies.

The adsorption – desorption isotherms obtained at 77 K under N₂ for the ZrCe-MOFs are shown in Figs. 1d and 2 d. The specific surface areas

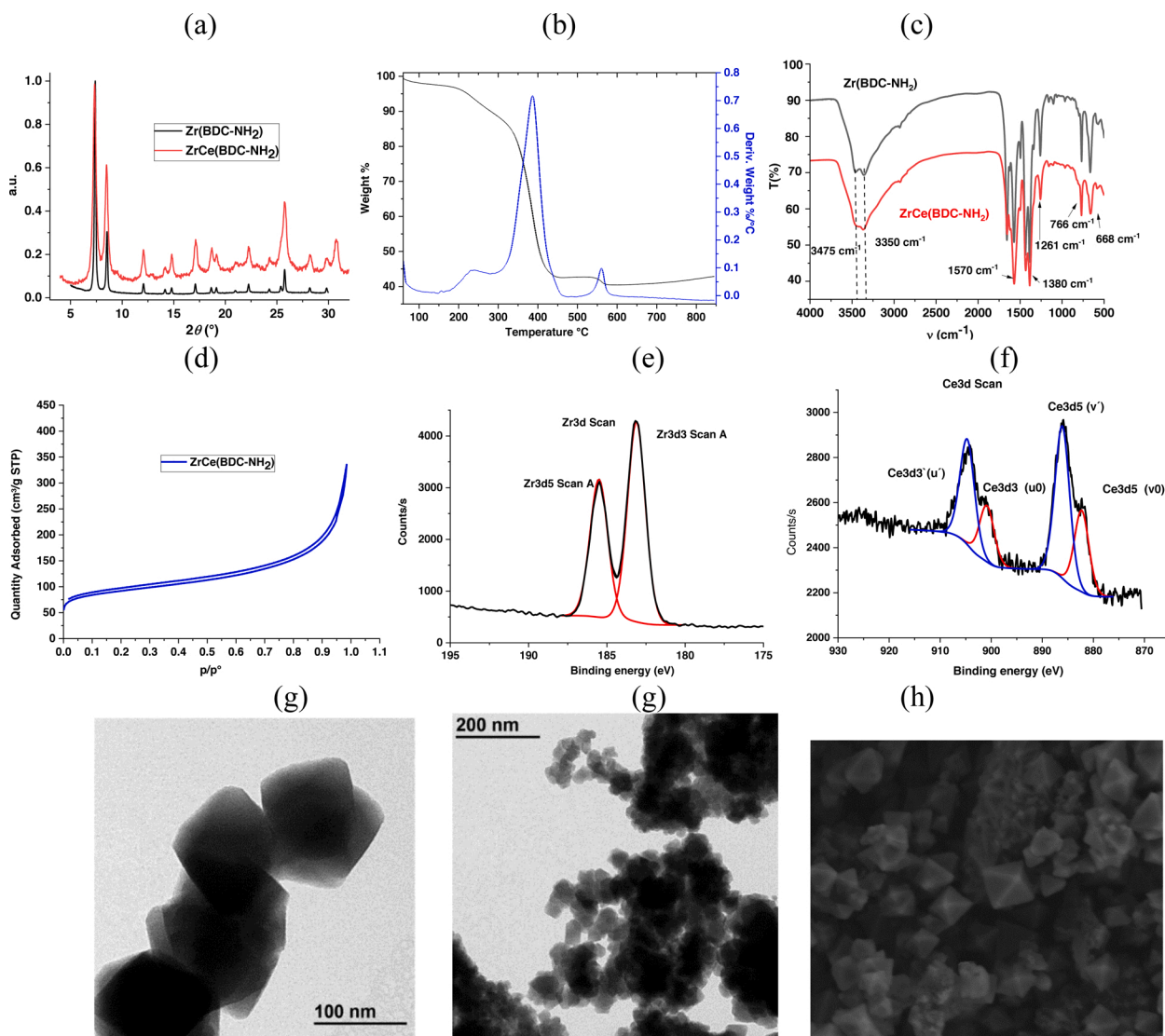


Fig. 1. Characterization data of ZrCe(BDC-NH₂): a) PXRD patterns; b) Thermal analysis; c) FT-IR spectra; d) N₂ isotherm; e, f) Zr and Ce region of XPS spectra; g) TEM images; h) SEM images.

were calculated by Brunauer – Emmett – Teller (BET) method, being 333 m² · g⁻¹ for ZrCe(BDC-NH₂), and 444 m² · g⁻¹ for ZrCe(NDC)(NDC-NH₂) with pore volumes of 0.45 and 0.34 cm³ · g⁻¹, respectively. The pores distribution is shown in Fig. S5.

In order to know in which oxidation state is the cerium into the samples, XPS analysis of mixed ZrCe-MOFs were performed (Figs. 1e, f, 2e, f, S6) and also from the recovered MOFs, as will be comment later (Fig. 6). The satellite peak located at the high binding energy (around 917 eV) associated to the Ce 3d_{3/2}, is characteristic of the presence of tetravalent Ce (Ce⁴⁺ ions) in Ce compounds. When tetravalent Cerium is abundant, the peak should be clearly visible. This satellite is not present in the samples. Therefore, we can conclude that the Ce³⁺ species is the most abundant in the material [23].

TEM images displayed in Figs. 1g and 2g show that ZrCe-MOFs have an irregular octahedral shape with the size ranging between 40 and 100 nm, similar to those reported previously. The morphology of all MOFs was also analyzed by SEM. Mixed MOFs adopts the typical octahedral geometry of UiO-66 structure (Figs. 1h, 2h). Ce MOFs, instead adopt the geometry of cubic rods (Fig. S7).

3.2. Evaluation of catalytic activity

3.2.1. Photocatalytic oxidation of benzylic alcohols

Heterogeneous photocatalysis has been largely studied due to its application in the environmental remediation and for obtaining renewable energy [65,66]. Different types of materials like supported metal nanoparticles [67], metal oxides based on bismuth [68] or titania [69], porous organic polymers (POPs) [70–74] or metal organic frameworks (MOFs) [75,76] have been applied as photocatalysts for the visible light aerobic oxidation of alcohols. MOFs have unique characteristics such as high porosity, tunability, well-defined structure and semiconductor properties, which make them perfect photocatalysts platforms for solving many environmental challenges [77,78,37,79]. Several approaches to increase the photocatalytic activity of certain MOFs, UiO-66 or ZIF-8 among others, have been reported by post-modification of the preformed MOF [80,81]. For example, the introduction of linkers with substituents such as NH₂ results in extending absorption in the visible spectrum [82–84]. This effect has been observed in our materials.

The photocatalytic performance depends on the light absorbing capability and the charge carrier separation efficiency, so the solid-state UV – vis absorption and diffuse reflectance spectra of Zr-based MOFs

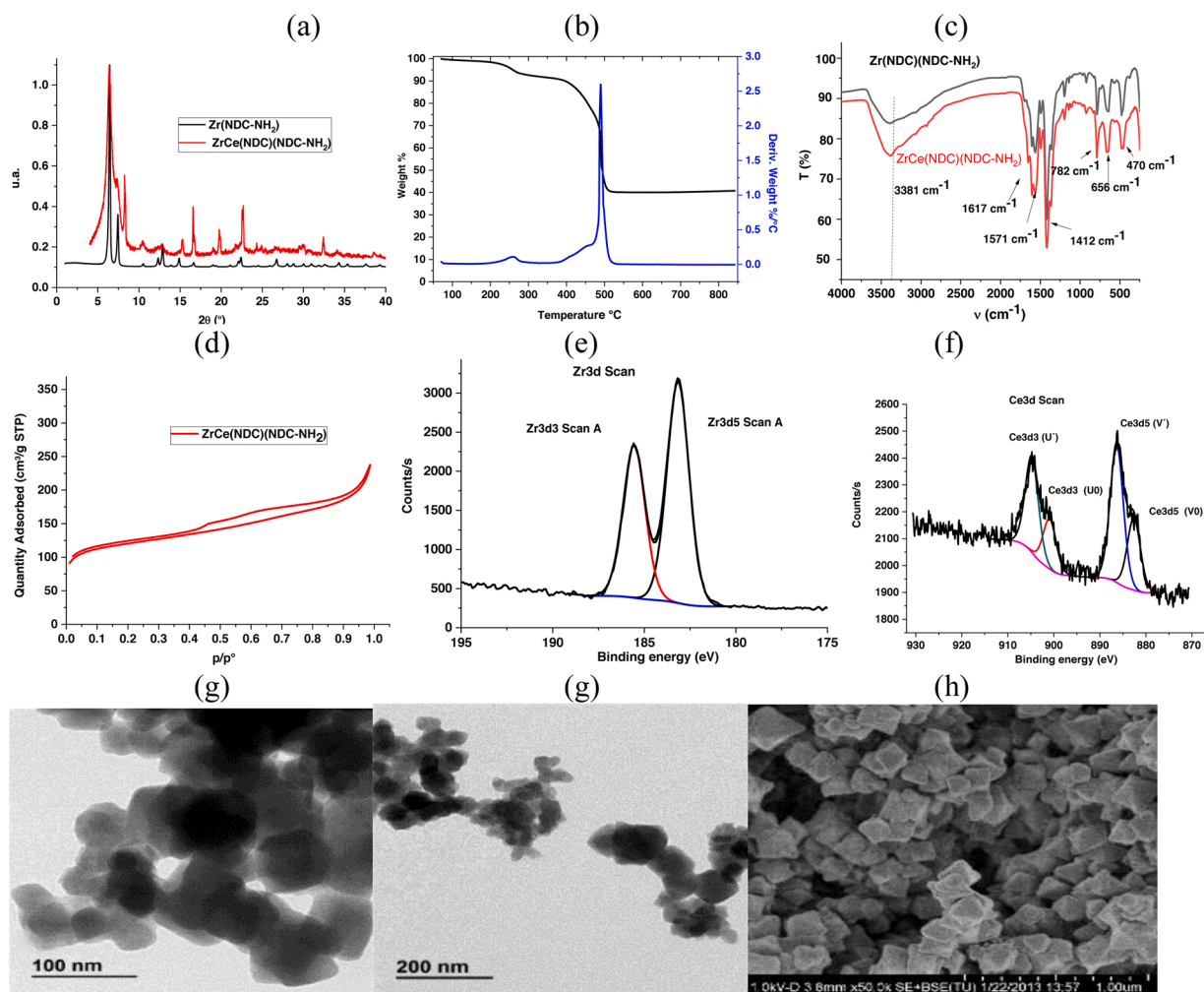


Fig. 2. Characterization data of ZrCe(NDC)(NDC-NH₂): a) PXRD patterns; b) Thermal analysis; c) FT-IR spectra; d) N₂ isotherm; e, f) Zr and Ce region of XPS spectra; g) TEM images; h) SEM images.

were investigated (Figs. 3a and S8) and the band gap energies λ_{abs} and E_{max} values estimated (Table 1). A comparison of spectra between, ZrCe-MOFs and their parent Zr- and Ce-based MOFs shows a shift to visible region, which implies a superior visible light absorption capacity. The

spectra show absorbance bands in the UV (290 nm), the near-vis (330, 350 nm) and visible region (~420 nm) which are associated with the chromophore NDC-NH₂ [85]. This shift to the visible light region is confirmed with the color changing from white to yellow for -NH₂

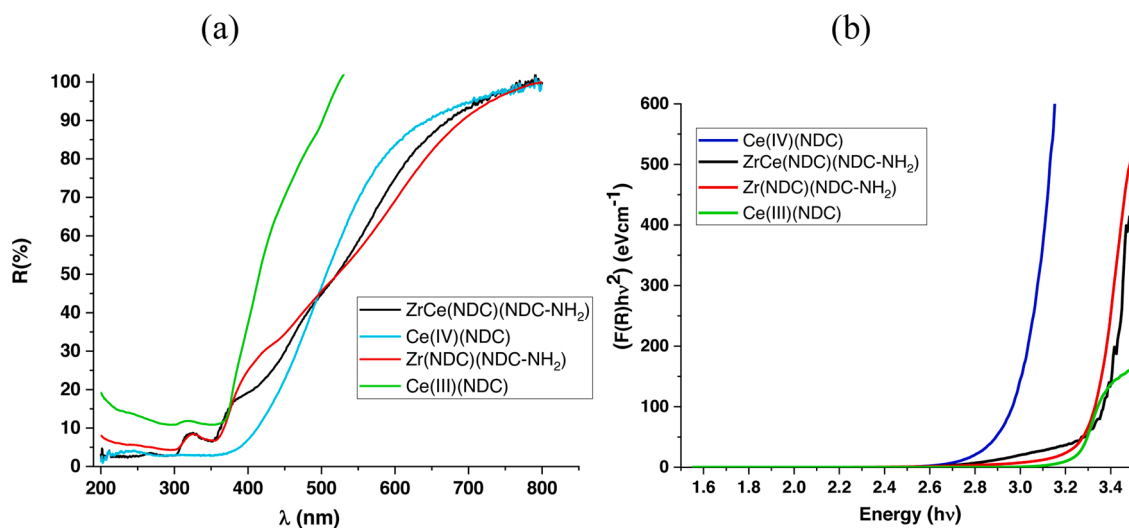


Fig. 3. (a) Reflectance diffuse spectra and (b) tauc plots for mixed ZrCe-, Zr- and Ce-MOFs.

Table 1

$E_{\text{band gap}}$ obtained from tauc plot and λ and E_{max} obtained from solid-state absorbance measurements.

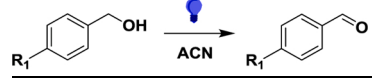
Material	$E_{\text{band gap}}$ (eV) ^a	λ_{abs} (nm)	E_{max} (eV) ^b ($\lambda \geq 350$ nm)
Zr(NDC)(NDC-NH ₂)	3.16	294, 333, 351, 417	2.97
ZrCe(NDC)(NDC-NH ₂)	3.10	297, 352, 420	2.95
Ce(III)(NDC)	3.13	300, 358, 433	2.86
Ce(IV)(NDC)	2.97	286, 350	3.54

^a Calculated from tauc plot.

^b Calculated from $E_g = \frac{1240 \text{ nm eV}}{\lambda_{\text{onset}} (\text{nm})}$.

derivatives. Band gap values were achieved using the Kubelka-Munk function from the tauc plots (Figs. 3b and S9) are estimated to be 3.16 eV for Zr(NDC)(NDC-NH₂) (2.75 for UiO-66-NH₂) [83,86], 3.10 eV for ZrCe(NDC)(NDC-NH₂), 2.97 eV for Ce(IV)(NDC) (2.82 eV for Ce-UiO-66) [81] and 3.13 eV for Ce(III)(NDC). The reported spectroscopic and photodynamics data of Zr(NDC)(NDC-NH₂) MOFs in the fs to ms scale, show that it occurs an energy transfer from excited NDC to NDC-NH₂ linkers and also a ligand-to cluster charge transfer (LCCT) process upon their photoexcitation. This LCCT process along with the separation of electrons and holes in the excited state indicates that MOFs can reduce or oxidize organic dyes [87,88].

Having confirmed the absorption's shift to the visible region of our NH₂-materials, we evaluated their photocatalytic activity in the oxidation of benzylic alcohols to their corresponding aldehydes under the irradiation of visible light (LED blue lamp, 50 w, $\lambda \geq 420$ nm) and results are summarized in Table 2. For these photocatalytic tests, BDC-NH₂ based MOFs have not been employed since they have been widely exploited and we have only focus on the less employed linker NDC-NH₂. To remove water and solvent molecules adsorbed on the surface, all materials were heated at 120 °C for 2 h under vacuum. As model substrate, 4-methoxybenzyl alcohol was chosen and reaction performed in acetonitrile resulting that ZrCe(NDC)(NDC-NH₂) is an efficient photocatalyst to selectively oxidize the alcohol to 4-methoxybenzaldehyde yielding 80 % conversion at 24 h reaction time, being complete at 48 h (entry 1). In addition, it results active and selective for the oxidation of

Table 2
Photocatalytic oxidation of benzylic alcohols.^a


Entry	Photocatalyst	R	Conv. (%) ^b	
			24 h	48 h
1	ZrCe(NDC)(NDC-NH ₂)	4-MeO	80	98
2		4-Me	35	55
3		4-Cl	45	95
4		H	30	50
5	Zr(NDC)(NDC-NH ₂)		99	–
6	Ce(III)(NDC)	4-	–	20
7	Ce(IV)(NDC)	MeO	< 5	–
8 ^b	Ce(IV)(NDC)/TEMPO ^c		18	37
9	Zr-UiO66-NH ₂ [84]		18	–
10	UiO66-NH ₂ [83] ($\lambda \geq 420$ nm, O ₂)		11.1(12 h)	–
11	UiO-66(NH ₂) [85] ($\lambda \geq 420$ nm, 0.1 MPa O ₂)	H	21.2 (4 h)	–
12	Ce-UiO-66-H [89] ($\lambda = 355 \pm 20$ nm, O ₂ flux)		95 (1.5 h)	–

^a Reaction conditions: 0.08 mmol alcohol, acetonitrile (1.5 mL), xylene as standard, 20 mg cat., blue LED lamp ($\lambda \geq 420$ nm, 50 W).

^b The corresponding aldehyde is selectively obtained.

^c 1.2 Eq of TEMPO.

different benzylic alcohols to the corresponding aldehydes. Thus, 4-methylbenzyl alcohol (electron-donating group) gives 55 % conversion at 48 h (entry 2); benzylic alcohols with electron-accepting groups, such as Cl, were also converted selectively (conversion >95 % at 48 h, entry 3). Unsubstituted benzyl alcohol (entry 4) gives less conversion. Zr(NDC)(NDC-NH₂) (entry 5) is the most active photocatalyst for the oxidation of *p*-methoxybenzyl alcohol leading the corresponding aldehyde quantitatively and selectively in 24 h.

As commented in the previous section, ZrCe(NDC)(NDC-NH₂) is obtained accompanied of a small amount of Ce(III)(NDC) with a FJU-6 structure. To evaluate the role of this phase, photooxidation experiments were performed with Ce(III)(NDC) and, for comparative purposes, with Ce(IV)(NDC); only traces of aldehyde were obtained in both cases (Table 2, entries 6 and 7). If TEMPO was added to the reaction media (entry 8), 37 % of desired product was obtained after 48 h reaction time, this is due to the synergic effect between Ce(IV) and TEMPO described by De Vos et al. when studying the same reaction [17]. Introduction of cerium in the clusters modifies the density of states' distribution (DES) of the resulting mixed MOF which in our conditions seems to negatively affect to the photocatalytic activity, being ZrCe(NDC)(NDC-NH₂) less active than pure Zr(NDC)(NDC-NH₂). Comparisons with the literature data (Table 2, entries 9–12), led to confirm that ZrCe- and Zr(NDC)(NDC-NH₂) are efficient and competitive photocatalysts under blue LED light, showing high yields at relatively shorter reaction times.

A series of control experiments were carried out to validate the photocatalytic process (Table 3). Reactions without photocatalyst (entry 2) or in light absence (entry 3) lead to negligible conversions that confirms the photocatalytic nature of the reaction. To discard the thermal catalytic reaction, an experiment was also carried out at 60 °C without light, obtaining 10 % of aldehyde after 48 h (entry 4), which confirms the oxidation of benzylic alcohols is mainly photocatalytic. Reaction in absence of oxygen atmosphere shows that only 40 % conversion (entry 5) is obtained after 48 h, indicating that oxygen is the main oxidant for the photocatalytic oxidation. It can be also observed that reaction in ethanol (a hole scavenger) inhibits the conversion of benzylic alcohol (entry 6). Additionally, Zr(NDC) only gives 18 % conversion after 48 h reaction time under the same conditions (entry 7), confirming the unique role of the amine groups. Reaction in presence of amino-linker only yields traces of aldehyde (entry 8). These last two experiments along with the experiments performed with the pure cerium MOFs, led to conclude that it is the combination of zirconium nodes with NDC-NH₂ linker, what makes the charge separation suitable for this reaction following a similar mechanism to that previously described using Zr-UiO66-NH₂ [37,83–85]. Thus, under visible light irradiation, the electrons from the HOMO of the amine-linker were excited to the LUMO level and moved to oxygen molecules adsorbed on the zirconium sites to form radicals (O₂^{•-}). On the other hand, the photogenerated holes oxidize the organic reactive substrates adsorbed on the amine groups (on the linkers) to carbonium ions. The O₂^{•-} radicals further react with the

Table 3
Control experiments of the photocatalytic oxidation.^a

Entry	Photocatalyst	Conditions	Conv. (%) (h)
1	ZrCe(NDC)(NDC-NH ₂)	Standard	80 (24)
2	none	Standard	Traces (24)
3	ZrCe(NDC)(NDC-NH ₂)	Dark	< 6 (48)
4	ZrCe(NDC)(NDC-NH ₂)	without light/60 °C	10 (48)
5	ZrCe(NDC)(NDC-NH ₂)	without O ₂	40 (48)
6	ZrCe(NDC)(NDC-NH ₂)	In EtOH	61 (42)
7	Zr(NDC)	Standard	18 (24)
8	NDC-NH ₂	Standard	Traces (24)
9	Ce(III)(NDC)	Standard	20 (48)
10	Ce(IV)(NDC)	Standard	<5 (24)

^a Standard reaction conditions: alcohol (0.08 mmol), acetonitrile (1.5 mL), standard (xylene), cat. (20 mg), blue LED lamp ($\lambda \geq 420$ nm, 50 W).

benzylic cations, which leads to the final oxidize products.

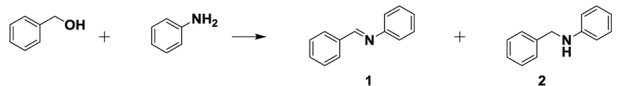
The reusability of the photocatalysts was evaluated in successive runs after washing and drying the solid after each cycle (Fig. 4). Photocatalytic selective oxidation of 4-methoxybenzyl alcohol is maintained over 4 cycles, after that, some activity is lost which remains over 3 cycles more. It seems that some photocatalyst mass is lost in the successive washes and perhaps products would remain on the photocatalyst and blockage the active sites. Inductively coupled plasma optical emission spectroscopy (ICP-OES) analysis of filtrate confirms that there has been no leaching. Fig. S10 displays the XRD patterns of the recovered ZrCe (NDC)(NDC-NH₂). Both samples, fresh and recovered photocatalysts, show similar XRD patterns and no significant differences have been observed after the reaction.

3.2.2. N-alkylation of amines with benzylic alcohols

The direct synthesis of imines from alcohols and amines is already described with Ag supported on γ -Alumina [90], Cu/Al hydrotalcite [91], Ru [92], or Ru and Au heterogenized polymers [93] and in presence of CeO₂-based materials as catalysts [94–97]. Imines are used in organic synthesis as intermediates for the synthesis of nitrogen containing heterocycles [98]. In this paper, we have evaluated the catalytic activity of mixed ZrCe-MOFs for the N-alkylation of amines with benzylic alcohols and results are displayed in Tables 4 and 5. For comparative purpose, pure cerium MOFs were also tested to evaluate the influence of the cerium(III) in the catalytic activity. In recent years, N-alkylamines synthesis from anilines and alcohols under visible light were reported over transition metals-MOF-catalysts and a base as additive [99,100].

Thus, considering the obtained results for photocatalytic oxidation of benzyl alcohols by Zr and ZrCe-MOFs described before, in a second part of the work, we have applied them to catalyze the N-alkylation of aniline with benzyl alcohol under visible light in acetonitrile without an external base (Table 4, entries 1 and 2). In this case, only traces of the corresponding imine are observed after 24 h being necessary very long reaction times to obtain acceptable yields. Thus, we opted to explore other conditions as typical thermal conditions; however, extended reaction times were also necessary to achieve good conversions (Table 4, entry 3). As an alternative, we have applied microwaves activation, which considerably decreases the reaction time to obtain good yields (Table 4, entry 4) (similar conditions were employed for MW-assisted SmI₂-catalyzed reaction [101]). In this case, both ZrCe-MOFs show similar activity yielding selectively N,1-diphenylmethanimine (entries 4, 5). Under similar conditions, the catalytic system formed by pure

Table 4
Synthesis of imines from alcohols and amines catalyzed by ZrCe-MOFs.



Entry	Catalyst	Conditions	Conv. (%) (h) ^d	Sel. (%) ^d		
				1	2	
<i>Photochemical activation</i>						
1	ZrCe(NDC)(NDC-NH ₂)	Blue light ^a	traces (24)	100	–	
2	Zr(NDC)(NDC-NH ₂)			100	–	
<i>Thermal activation</i>						
3	ZrCe(NDC)(NDC-NH ₂)	150 °C ^b	76 (48)	98	2	
4	ZrCe(NDC)(NDC-NH ₂)	MW ^c	84 (8)	91	9	
5	ZrCe(BDC-NH ₂)		75 (8)	94	6	
6	Ce(III)NDC/KOtBu		99 (3)	3	97	
7	Ce(IV)NDC/KOtBu		99 (3)	15	85	
<i>Control experiments</i>						
8	Ce(III)NDC	MW ^c	traces (3)	–	–	
9	CeCl ₃ /KOtBu			50 (3)	100	–
10	Zr(NDC)			traces (8)	–	–
11	Zr(NDC)/KOtBu		90(10)	100	0	
12	–		traces			

^a Photochemical conditions: alcohol (0.2 mmol), 0.1 mmol of amine, acetonitrile (1.5 mL), cat. (20 mg), blue LED lamp ($\lambda \geq 420$ nm, 50 W).

^b Reaction performed under conventional heating at 150 °C.

^c MW reaction conditions: 0.2 mmol of alcohol and 0.1 mmol of amine were dissolved in 0.5 mL of xylene, 10 mg of catalyst was added, and the reaction mixture was introduced on a MW (150 °C).

^d Determined by GC-MS.

cerium MOFs and KOtBu (as external base) selectively leads to N-benzylaniline (entries 6, 7). Control experiments show that the reaction catalyzed by MOFs prepared with NDC ligand (without amine groups) as Ce(III)(NDC) (entry 8) or Zr(NDC) (entry 10) or in absence of catalyst (entry 12) only yields traces of the product. As it is well known, the formation of imine from aniline and benzaldehyde is fast; therefore, the formation of imine catalyzed by Zr(NDC) in presence of KOtBu (entry 11) indicated that base additive had a significant effect on the benzyl alcohol oxidation to benzaldehyde. Reaction with the system commercial CeCl₃/KOtBu gives the imine with a 50 % yield (entry 9).

The scope of the reaction was analyzed with different alcohols and amines (Table 5). In general, mixed ZrCe-catalysts leads to the imine as main product and only traces of the corresponding secondary amine were obtained and ZrCe(BDC-NH₂) showed better reactivity than ZrCe

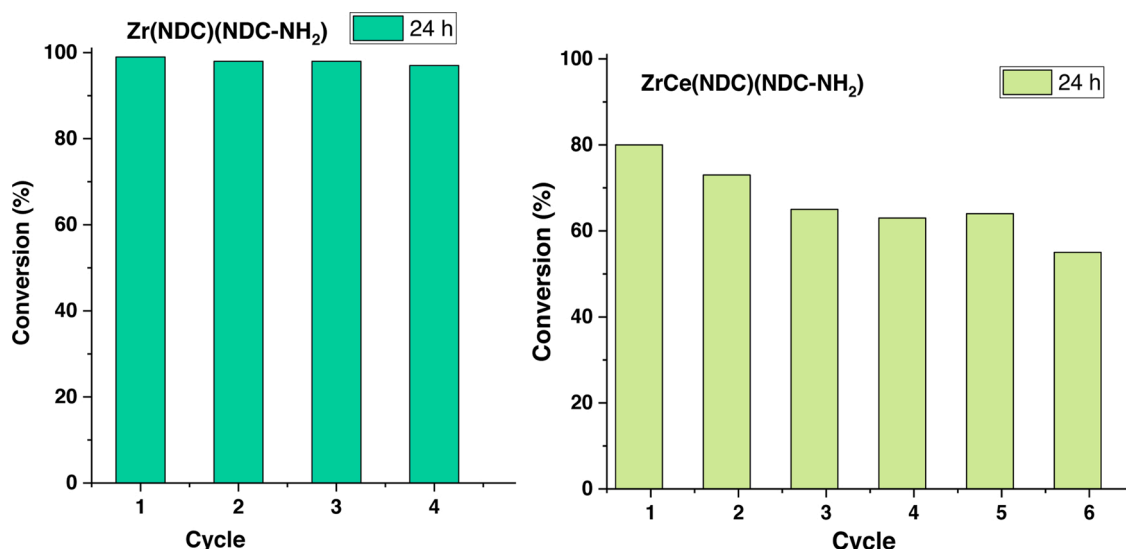
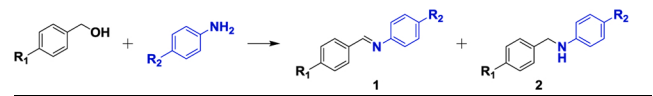


Fig. 4. Recycling experiments for the photocatalytic oxidation of 4-methoxybenzyl alcohol.

Table 5
Synthesis of imines from alcohols and amines catalyzed by ZrCe-MOFs.^a



Entry	Catalyst	R1	R2	Conv. (%) (h) ^b	Sel. (%) ^b	
					1	2
1	ZrCe(BDC-NH ₂)	OCH ₃	H	90 (8)	82	18
2		CH ₃	H	99 (8)	93	7
3		Cl	H	62 (8)	100	–
4	ZrCe(NDC)(NDC-NH ₂)	OCH ₃	H	80 (8)	62	38
5		CH ₃	H	15 (8)	100	–
6		Cl	H	37 (8)	100	–
7		H	Br	9 (8)	100	–
8	Ce(III)NDC/KOtBu	OCH ₃	H	100 (3)	20	80
9		H	Br	85 (3)	15	85

^a Reaction conditions: 0.2 mmol of alcohol and 0.1 mmol of amine were dissolved in 0.5 mL of xylene, 10 mg of catalyst was added, and the reaction mixture was introduced on a MW (150 °C).

^b Determined by GC-MS.

(NDC)(NDC-NH₂). Reaction with (4-methoxyphenyl)methanol as substrate yields 18 % and 38 % of the corresponding amine (entries 1 and 4), indicating that electronic factors of the resulting imine bond might enable its subsequent hydrogenation. If alcohols or amines with electron withdrawing groups at the aromatic ring are used (entries 3, 6, 7) the conversion is lower, being more pronounced in the case of substituents over the aromatic ring of the amine (entry 7). Besides, when the catalytic system CeMOFs/ KOtBu is employed, the secondary amine is obtained as the main product (entries 8 and 9).

The scope of the reaction with cerium-MOFs as catalysts was also evaluated (Table S2). Both cerium MOFs selectively yields the

corresponding amine when we reacted benzyl alcohol and 4-methoxyaniline (entries 1 and 4). Again, it is observed, that the nature of the imine bond plays a key role in the selectivity towards the secondary amine, as it happened with ZrCe-MOFs. Thus, non-conjugated imines seem to be less likely to be hydrogenated (entries 2, 3, 5 and 6).

A series of control experiments were done to evaluate the role of cerium in the *N*-alkylation reaction (Scheme S1). We think that in the presence of the corresponding MOF and KOt-Bu dehydrogenation of a primary alcohol gives the corresponding aldehyde, which subsequently reacts with the amine to form the imine intermediate. Further, cerium clusters reduce the imine intermediate affording the amine product, unlike pure Zr-MOFs which only affords the corresponding imine. Thus, we suggest the formation of a cerium-hydride as the active species since analogous behavior has been described with a samarium catalyst in the same reaction [101]. Furthermore, the existence of a Ce-H species has been already described for a Ce-BTC MOF (BTC = benzene tricarboxylate) [102].

The scaled up by a factor of 10 was carried out with both catalysts, in presence of ZrCe(BDC-NH₂) a conversion of 60 % was obtained after 8 h of reaction with a selectivity of 93 % towards the imine. Recycling experiments were carried out and showed that the activity remains without significant loss up to six runs (Fig. 5). After each run, the solid was separated from the reaction mixture by filtration, thoroughly washed and dried at 100 °C under vacuum for 1–2 h. Analysis of the reaction liquid using ICP-OES showed that metal leaching is very low (<1%) and hot filtration experiments demonstrates that there are no active species in the reaction liquid (Fig. S14). X-ray diffraction pattern of recovered solid shows that the structure is maintained after six cycles (Fig. S11) and XPS analysis showed that the Ce³⁺ species are still the most abundant in the structure since the satellite around 917 eV is not observed in the spectra (Fig. 6). XPS survey scan of both ZrCe-MOFs is shown in Fig. S12. The N₂ sorption experiments of samples post-catalysis

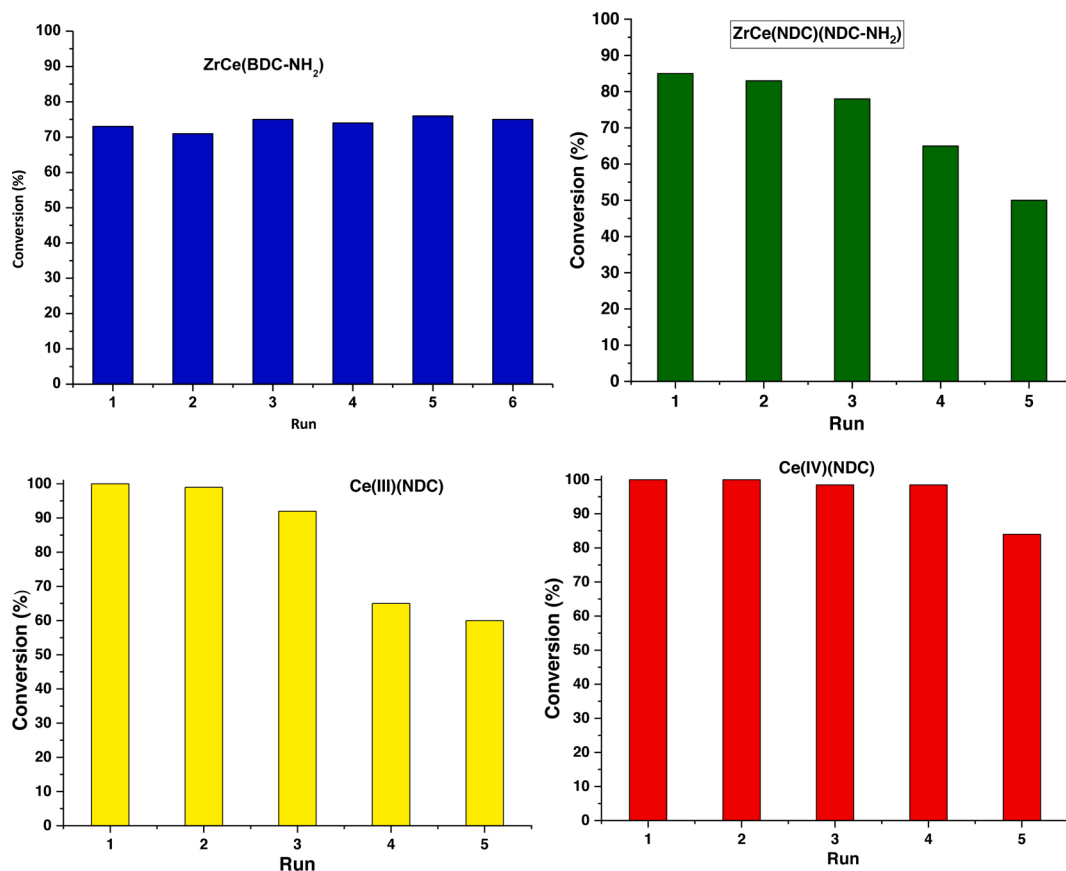


Fig. 5. Recycling experiments.

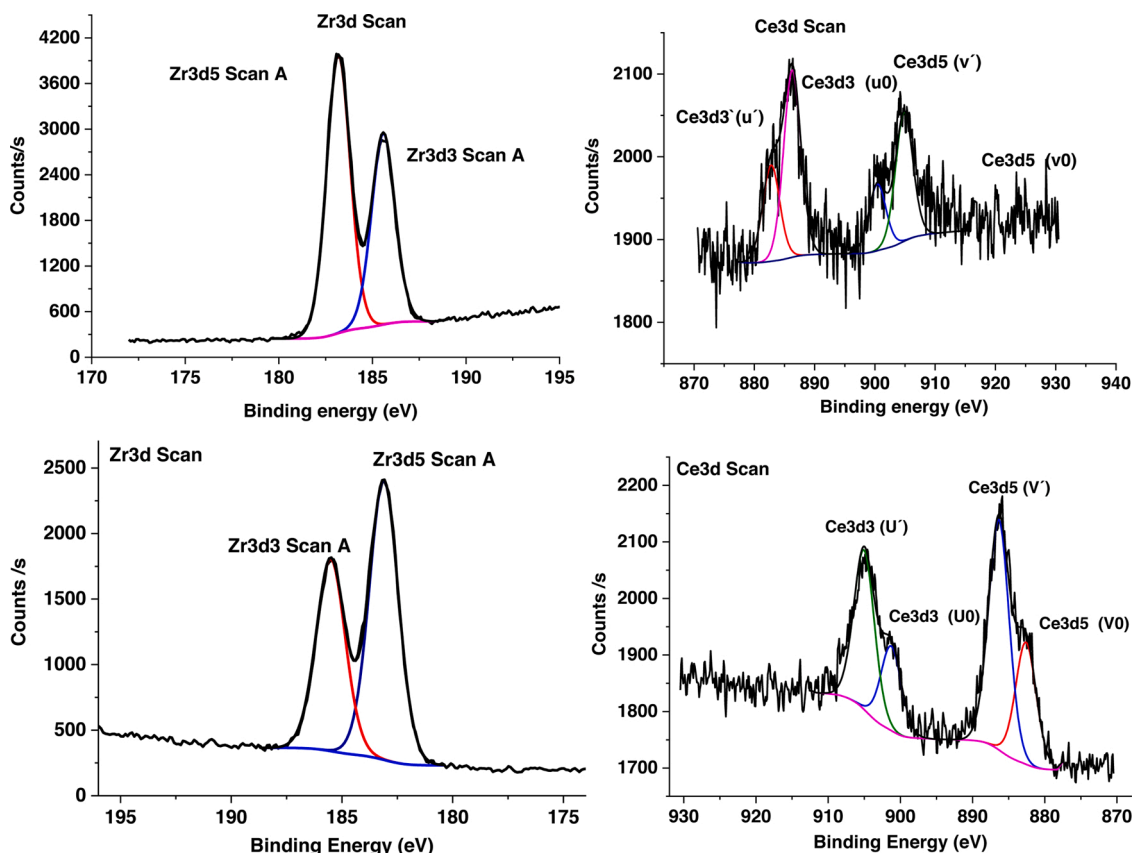


Fig. 6. Zr and Ce region of XPS spectra of recovered ZrCe(BDC-NH₂) (top) and ZrCe(NDC)(NDC-NH₂) (down).

show that a BET surface area is slightly less than fresh catalyst (265 and 395 m²·g⁻¹), probably due to reagents and products trapped in the material (Fig. S13).

Cerium(III)(NDC) seem to be less stable than Ce(IV)(NDC) and ZrCe(BDC-NH₂), since a decrease in activity for successive runs when ZrCe(NDC)(NDC-NH₂) and Ce(III)(NDC) are employed as catalysts (Fig. 5). However, Ce(IV)(NDC) maintains its activity at least for four consecutive runs. XRD of the 5th-cycle shows that the crystallinity of Ce(IV)(NDC) has decreased, even though its pattern remains similar, whereas Ce(III)(NDC) results amorphous (Fig. S11). This also probes that zirconium nodes afford stability and increases its robustness in this catalytic system, in contrast to Ce(III) nodes which seems to be weaker. Hot filtration experiments were also carried out showing that catalysts were heterogeneous and recyclable for several runs (Fig. S14). The selectivity towards the amine does also decrease with the subsequent cycles.

4. Conclusion

In summary, we report that amino-functionalized non-noble-metal-based heterogeneous catalysts, Zr-, ZrCe- and Ce-MOFs, were obtained and evaluated as heterogeneous catalysts. In the first part, Zr- and ZrCe(NDC)(NDC-NH₂) result efficient photocatalysts for the oxidation of benzylic alcohols under visible light irradiation, whereas materials that do not contain amino ligands, did not catalyze the reaction. Moreover, they exhibit high stability and considerable recyclability. In the second part, we study the *N*-alkylation of amines with benzyl alcohols under microwaves activation resulting that Zr-materials afforded mainly imines whereas Ce-compounds selectively give secondary amines. The catalysts maintain their activity up to six cycles without significant loss of activity.

CRediT authorship contribution statement

Antonio Valverde-González, Mercedes Pintado-Sierra, Antonia Rasero-Almansa: Design, experimental work, and manuscript writing and correction **Félix Sánchez and Marta Iglesias:** Conceptualization and Design the whole study, manuscript writing and proofreading of the manuscript.

Declaration of Competing Interest

The authors declare that they have no known competing financial interests or personal relationships that could have appeared to influence the work reported in this paper.

Acknowledgments

Authors acknowledge to MINECO of SpainMAT2017-82288-C2-2-P project for financial support. A.V.G. thanks Ministerio de Educación y Formación Profesional for FPU17/03463. M.P.S thanks to MINECO of Spain for RTI2018-096328-B-I00 project.

Appendix A. Supplementary data

Supplementary material related to this article can be found, in the online version, at doi:<https://doi.org/10.1016/j.apcata.2021.118287>.

References

- [1] H. Furukawa, K.E. Cordova, M. O'Keeffe, O.M. Yaghi, *Science* 341 (2013), 1230444.
- [2] G. Férey, *Chem. Soc. Rev.* 37 (2008) 191–214.
- [3] O.M. Yaghi, H. Li, C. Davis, D. Richardson, T.L. Groy, *Acc. Chem. Res.* 31 (1998) 474–484.

- [4] V. Bernales, M.A. Ortuño, D.G. Truhlar, C.J. Cramer, L. Gagliardi, *ACS Cent. Sci.* 4 (2018) 5–19.
- [5] Y.B. Huang, J. Liang, X.S. Wang, R. Cao, *Chem. Soc. Rev.* 46 (2017) 126–157.
- [6] D. Yang, B.C. Gates, *ACS Catal.* 9 (2019) 1779–1798.
- [7] F.X. Llabrés i Xamena, J. Gascón, *Metal Organic Frameworks as Heterogeneous Catalysts*, Cambridge Royal Society of Chemistry, 2013.
- [8] T. Drake, P. Ji, W. Lin, *Acc. Chem. Res.* 51 (2018) 2129–2138.
- [9] L. Zhu, X.Q. Liu, H.L. Jiang, L.B. Sun, *Chem. Rev.* 117 (2017) 8129–8176.
- [10] J. Liu, Z. Li, X. Zhang, K.I. Otake, L. Zhang, A.W. Peters, M.J. Young, N. M. Bedford, S.P. Letourneau, D.J. Mandia, J.W. Elam, O.K. Farha, J.T. Hupp, *ACS Catal.* 9 (2019) 3198–3207.
- [11] J. Liu, L.R. Redfern, Y. Liao, T. Islamoglu, A. Atilgan, O.K. Farha, J.T. Hupp, *ACS Appl. Mater. Interfaces* 11 (2019) 47822–47829.
- [12] J.H. Cavka, S. Jakobsen, U. Olsbye, N. Guillou, C. Lamberti, S. Bordiga, K. P. Lillerud, *J. Am. Chem. Soc.* 130 (2008) 13850–13851.
- [13] R. Zhao, L. Shi, *Org. Chem. Front.* 5 (2018) 3018–3021.
- [14] A. Hu, J.J. Guo, H. Pan, Z. Zuo, *Science* 361 (2018) 668–672.
- [15] S. Smolders, A. Struyf, H. Reinsch, B. Bueken, T. Rhauderwiek, L. Mintrop, P. Kurz, N. Stock, D.E. De Vos, *Chem. Commun.* 54 (2018) 876–879.
- [16] M. Lammert, C. Glißmann, H. Reinsch, N. Stock, *Cryst. Growth Des.* 17 (2017) 1125–1131.
- [17] M. Lammert, M.T. Wharmby, S. Smolders, B. Bueken, A. Lieb, K.A. Lomachenko, D. De Vos, N. Stock, *Chem. Commun.* 51 (2015) 12578–12581.
- [18] X.P. Wu, L. Gagliardi, D.G. Truhlar, *J. Am. Chem. Soc.* 140 (2018) 7904–7912.
- [19] R. Dalapati, B. Sakthivel, A. Dhakshinamoorthy, A. Buragohain, A. Bhunia, C. Janiak, S. Biswas, *CrystEngComm* 18 (2016) 7855–7864.
- [20] J. Lyu, X. Zhang, P. Li, X. Wang, C.T. Buru, P. Bai, X. Guo, O.K. Farha, *Chem. Mater.* 31 (2019) 4166–4172.
- [21] P. Ji, T. Sawano, Z. Lin, A. Urban, D. Boures, W. Lin, *J. Am. Chem. Soc.* 138 (2016) 14860–14863.
- [22] V.R. Bakuru, S.R. Churipard, S.P. Maradur, S.B. Kalidindi, *Dalton Trans.* 48 (2019) 843–847.
- [23] Y. Xiong, S. Chen, F. Ye, L. Su, C. Zhang, S. Shen, S. Zhao, *Chem. Commun.* 51 (2015) 4635–4638.
- [24] R. D'Amato, A. Donnadio, M. Carta, C. Sangregorio, D. Tiana, R. Vivani, M. Taddei, F. Costantino, *ACS Sustain. Chem. Eng.* 7 (2019) 394–402.
- [25] J. Ethiraj, F. Bonino, J.G. Vitillo, K.A. Lomachenko, C. Lamberti, H. Reinsch, K. P. Lillerud, S. Bordiga, *ChemSusChem* 9 (2016) 713–719.
- [26] X. Wang, X. Zhang, P. Li, K.I. Otake, Y. Cui, J. Lyu, M.D. Krzyaniak, Y. Zhang, Z. Li, J. Liu, C.T. Buru, T. Islamoglu, M.R. Wasielewski, Z. Li, O.K. Farha, *J. Am. Chem. Soc.* 141 (2020) 8306–8314.
- [27] Y. Han, J.R. Li, Y. Xie, G. Guo, *Chem. Soc. Rev.* 43 (2014) 5952–5981.
- [28] S. Wongsakulphasatch, F. Nouar, J. Rodriguez, L. Scott, C. Le Guillouzer, T. Devic, P. Horcajada, J.M. Grenèche, P.L. Llewellyn, A. Vimont, G. Clet, M. Daturi, C. Serre, *Chem. Commun.* 51 (2015) 10194–10197.
- [29] K.A. White, D.A. Chengelis, K.A. Gogick, J. Stehman, N.L. Rosi, S. Petoud, *J. Am. Chem. Soc.* 131 (2009) 18069–18071.
- [30] A.M. Ebrahim, T.J. Bandoz, *ACS Appl. Mater. Interfaces* 5 (2013) 10565–10573.
- [31] F. Nouar, M.I. Breeze, B.C. Campo, A. Vimont, G. Clet, M. Daturi, T. Devic, R. I. Walton, C. Serre, *Chem. Commun.* 51 (2015) 14458–14461.
- [32] S. Waitschat, D. Fröhlich, H. Reinsch, H. Terraschke, K.A. Lomachenko, C. Lamberti, H. Kummer, T. Helling, M. Baumgartner, S. Henninger, N. Stock, *Dalton Trans.* 47 (2018) 1062–1070.
- [33] R. Di Monte, J. Kašpar, *J. Mater. Chem.* 15 (2005) 633–648.
- [34] Y.S. Wei, M. Zhang, R. Zou, Q. Xu, *Chem. Rev.* 120 (2020) 12089–12174.
- [35] A. Bavykina, N. Kolobov, I.S. Khan, J.A. Bau, A. Ramirez, J. Gascon, *Chem. Rev.* 120 (2020) 8468–8535.
- [36] J. Guo, Y. Qin, Y. Zhu, X. Zhang, C. Long, M. Zhao, Z. Tang, *Chem. Soc. Rev.* 50 (2021) 5366–5396.
- [37] A. Dhakshinamoorthy, Z. Li, H. García, *Chem. Soc. Rev.* 47 (2018) 8134–8172.
- [38] A. Dhakshinamoorthy, A.M. Asiri, H. Garcia, *Chem. Commun.* 53 (2017) 10851–10869.
- [39] M. Hao, Z. Li, *Sol. RRL* 5 (2021) 1–14.
- [40] Z. Hu, Y. Wang, D. Zhao, *Chem. Soc. Rev.* 50 (2021) 4629–4683.
- [41] N.B. Patel, N. Vala, A. Shukla, S. Neogi, M.K. Mishra, *Catal. Commun.* 144 (2020), 106085.
- [42] Y. Lin, C. Kong, L. Chen, *RSC Adv.* 6 (2016) 32598–32614.
- [43] M. Pintado-Sierra, A.M. Rasero-Almansa, A. Corma, M. Iglesias, F. Sánchez, *J. Catal.* 299 (2013) 137–145.
- [44] C.X. Chen, Z.W. Wei, J.J. Jiang, S.P. Zheng, H.P. Wang, Q.F. Qiu, C.C. Cao, D. Fenske, C.Y. Su, *J. Am. Chem. Soc.* 139 (2017) 6034–6037.
- [45] A. Khansari, M.R. Bryant, D.R. Jenkinson, G.B. Jameson, O.T. Qazvini, L. Liu, A. D. Burrows, S.G. Telfer, C. Richardson, *CrystEngComm* 21 (2019) 7498–7506.
- [46] M.S. Yazdanparast, V.W. Day, T. Gadzikwa, *Molecules* 25 (2020) 697.
- [47] A.M. Rasero-Almansa, A. Corma, M. Iglesias, F. Sánchez, *ChemCatChem* 6 (2014) 3426–3433.
- [48] S. Yuan, J.S. Qin, H.Q. Xu, J. Su, D. Rossi, Y. Chen, L. Zhang, C. Lollar, Q. Wang, H.L. Jiang, D.H. Son, H. Xu, Z. Huang, X. Zou, H.C. Zhou, *ACS Cent. Sci.* 4 (2018) 105–111.
- [49] J. Sim, H. Yim, N. Ko, S.B. Choi, Y. Oh, H.J. Park, S.Y. Park, J. Kim, *J. Chem. Soc. Dalton Trans.* 43 (2014) 18017–18024.
- [50] S.A. Diamantis, A. Hatzidimitriou, A.K. Plessas, A. Pournara, M.J. Manos, G. S. Papaefstathiou, T. Lazarides, *Dalton Trans.* 49 (2020) 16736–16744.
- [51] H. Imagawa, A. Suda, K. Yamamura, S. Sun, *J. Phys. Chem. C* 115 (2011) 1740–1745.
- [52] J. Jacobsen, A. Ienco, R. D'Amato, F. Costantino, N. Stock, *Dalton Trans.* 49 (2020) 16551–16586.
- [53] Q. Liu, H. Cong, H. Deng, *J. Am. Chem. Soc.* 138 (2016) 13822–13825.
- [54] F. Trouselet, A. Archereau, A. Boutin, F.X. Coudert, *J. Phys. Chem. C* 120 (2016) 24885–24894.
- [55] A. Melillo, M. Cabrero-Antonino, S. Navalón, M. Álvaro, B. Ferrer, H. García, *Appl. Catal. B Environ.* 278 (2020) 119345–119346.
- [56] A. Loosen, C. Simms, S. Smolders, D.E. De Vos, T.N. Parac-Vogt, *ACS Appl. Nano Mater.* 4 (2021) 5748–5757.
- [57] M. Ronda-Lloret, I. Pellicer-Carreño, A. Grau-Atienza, R. Boada, S. Diaz-Moreno, J. Narciso-Romero, J.C. Serrano-Ruiz, A. Sepúlveda-Escribano, E.V. Ramos-Fernandez, *Adv. Funct. Mater.* (2021), 2102582.
- [58] K.A. Lomachenko, J. Jacobsen, A.L. Bugaev, C. Atzori, F. Bonino, S. Bordiga, N. Stock, C. Lamberti, *J. Am. Chem. Soc.* 140 (2018) 17379–17383.
- [59] J. Jacobsen, H. Reinsch, N. Stock, *Inorg. Chem.* 57 (2018) 12820–12826.
- [60] Y.H. Liu, P.H. Chien, *CrystEngComm* 16 (2014) 8852–8862.
- [61] C. Atzori, K.A. Lomachenko, S. Øien-Ødegaard, C. Lamberti, N. Stock, C. Barolo, F. Bonino, *Cryst. Growth Des.* 19 (2019) 787–796.
- [62] G.C. Shearer, S. Chavan, J. Ethiraj, J.G. Vitillo, S. Svelle, U. Olsbye, C. Lamberti, S. Bordiga, K.P. Lillerud, *Chem. Mater.* 26 (2014) 4068–4071.
- [63] M. Lammert, C. Glißmann, N. Stock, *Dalton Trans.* 46 (2017) 2425–2429.
- [64] B. Preetha, C. Janardanan, *Res. J. Recent Sci.* 1 (2012) 85–92.
- [65] C. Dai, B. Liu, *Energy Environ. Sci.* 13 (2020) 24–52.
- [66] C. Chen, W. Ma, J. Zhao, *Chem. Soc. Rev.* 39 (2010) 4206–4219.
- [67] Y. Chen, Y. Wang, W. Li, Q. Yang, Q. Hou, L. Wei, L. Liu, F. Huang, M. Ju, *Appl. Catal. B Environ.* 210 (2017) 352–367.
- [68] T. Li, T. Kasahara, J. He, K.E. Dettelbach, G.M. Sammis, C.P. Berlinguette, *Nat. Commun.* 8 (2017) 6–10.
- [69] L. Yu, Y. Lin, D. Li, *Appl. Catal. B Environ.* 216 (2017) 88–94.
- [70] W. Huang, B.C. Ma, H. Lu, R. Li, L. Wang, K. Landfester, K.A.I. Zhang, *ACS Catal.* 7 (2017) 5438–5442.
- [71] H. Xu, X. Li, H. Hao, X. Dong, W. Sheng, X. Lang, *Appl. Catal. B Environ.* 285 (2021), 119796.
- [72] J.L. Shi, R. Chen, H. Hao, C. Wang, X. Lang, *Angew. Chem. - Int. Ed.* 59 (2020) 9088–9093.
- [73] X. Li, J.L. Shi, H. Hao, X. Lang, *Appl. Catal. B Environ.* 232 (2018) 260–267.
- [74] X. Li, H. Hao, X. Lang, *J. Colloid Interface Sci.* 593 (2021) 380–389.
- [75] S. Yuan, T.F. Liu, D. Feng, J. Tian, K. Wang, J. Qin, Q. Zhang, Y.P. Chen, M. Bosch, L. Zou, S.J. Teat, S.J. Dalgarno, H.C. Zhou, *Chem. Sci.* 6 (2015) 3926–3930.
- [76] A. Dhakshinamoorthy, A.M. Asiri, H. Garcia, *Chem. Commun.* 53 (2017) 10851–10869.
- [77] Y. Zhang, J. Guo, L. Shi, Y. Zhu, K. Hou, Y. Zheng, Z. Tang, *Sci. Adv.* 3 (2017), e1701162.
- [78] L. Jiao, Y. Wang, H.L. Jiang, Q. Xu, *Adv. Mater.* 30 (2018) 1703663–1703686.
- [79] W. Zhan, L. Sun, X. Han, *Nano-Micro Lett.* 11 (2019) 1–28.
- [80] K. Hendrickx, J.J. Joos, A. De Vos, D. Poelman, P.F. Smet, V. Van Speybroeck, P. Van Der Voort, K. Lejaeghere, *Inorg. Chem.* 57 (2018) 5463–5474.
- [81] X.P. Wu, L. Gagliardi, D.G. Truhlar, *J. Am. Chem. Soc.* 140 (2018) 7904–7912.
- [82] X. Qiu, Y. Zhu, X. Zhang, Y. Zhang, L.T. Menisa, C. Xia, S. Liu, Z. Tang, *Sol. RRL* 4 (2020) 1900449–1900456.
- [83] C.G. Silva, A. Corma, H. García, *J. Mater. Chem.* 20 (2010) 3141–3156.
- [84] J. Long, S. Wang, Z. Ding, S. Wang, Y. Zhou, L. Huang, X. Wanga, *Chem. Commun.* 48 (2012) 11656–11658.
- [85] T.W. Goh, C. Xiao, R.V. Maligal-Ganesh, X. Li, W. Huang, *Chem. Eng. Sci.* 124 (2015) 45–51.
- [86] L. Shen, S. Liang, W. Wu, R. Liang, L. Wu, *Dalton Trans.* 42 (2013) 13649–13657.
- [87] M. Gutiérrez, F. Sánchez, A. Douhal, *Chem. - A Eur. J.* 22 (2016) 13072–13082.
- [88] M. Gutiérrez, B. Cohen, F. Sánchez, A. Douhal, *Phys. Chem. Chem. Phys.* 18 (2016) 27761–27774.
- [89] M. Campanelli, T. Del Giacco, F. De Angelis, E. Mosconi, M. Taddei, F. Marmottini, R. D'Amato, F. Costantino, *ACS Appl. Mater. Interfaces* 11 (2019) 45031–45037.
- [90] K. Shimizu, M. Nishimura, A. Satsuma, *ChemCatChem* 1 (2009) 497–503.
- [91] P.R. Likhari, R. Arundhathi, M.L. Kantam, P.S. Prathima, *Eur. J. Org. Chem.* (2009) 5383–5389.
- [92] V.R. Jumde, L. Gonsalvi, A. Guerriero, M. Peruzzini, M. Taddei, *Eur. J. Org. Chem.* 2015 (2015) 1829–1833.
- [93] A. Valverde-González, G. Marchal, E.M. Maya, M. Iglesias, *Catal. Sci. Technol.* 9 (2019) 4552–4560.
- [94] M. Tamura, K. Tomishige, *Angew. Chem. - Int. Ed.* 54 (2015) 864–867.
- [95] M. Zhang, S. Wu, L. Bian, Q. Cao, W. Fang, *Catal. Sci. Technol.* 9 (2019) 286–301.
- [96] L. Geng, J. Song, Y. Zhou, Y. Xie, J. Huang, W. Zhang, L. Peng, G. Liu, *Chem. Commun.* 52 (2016) 13495–13498.
- [97] Y. Long, H. Zhang, Z. Gao, J. Qin, Y. Pan, J. Zhao, Y. Luo, Z. Ma, Y. Xiong, J. Ma, *Inorg. Chem. Front.* 6 (2019) 829–836.
- [98] B. Chen, L. Wang, S. Gao, *ACS Catal.* 5 (2015) 5851–5876.
- [99] H. Cheng, X. Long, F. Bian, C. Yang, X. Liu, H. Jiang, *J. Catal.* 389 (2020) 121–131.
- [100] D. Wang, J. Albero, H. García, Z. Li, *J. Catal.* 349 (2017) 156–162.
- [101] J. Gour, S. Gatadi, S. Malasala, M.V. Yaddanpudi, S. Nanduri, *J. Org. Chem.* 84 (2019) 7488–7494.
- [102] P. Ji, T. Sawano, Z. Lin, A. Urban, D. Boures, W. Lin, *J. Am. Chem. Soc.* 138 (2016) 14860–14863.